

# Observational Constraints on Non-monotonic Infrared Emissions: Integrating Gaia–WISE Data with Thermodynamic Signature Boundary Conditions (TSBC)

Minjun Kim

*Independent Researcher*

---

## Abstract

Traditional searches for advanced technosignatures have largely focused on the detection of macroscopic waste heat, typically modeled as a smooth infrared (IR) excess associated with large-scale energy consumption. However, this assumption may break down if highly advanced civilizations evolve toward extreme thermodynamic efficiency. In such a regime, increasing total power consumption does not necessarily imply increasing observable waste heat; instead, dissipation may become spatially localized, spectrally selective, or non-monotonic across mid-infrared bands. In this paper, we formulate the *Thermodynamic Signature Boundary Condition* (TSBC) as an interpretive framework linking energy use, efficiency, radiative limits, and observability. We then integrate Gaia astrometry, WISE mid-infrared photometry, and SIMBAD cross-identification into an observational pipeline designed to detect non-uniform thermal structures. We derive angular-to-physical conversion relations, magnitude-to-flux transformations, band-limited luminosity proxies, local density statistics, and Poisson-based isolation tests to evaluate whether anomalous IR structures can be distinguished from common astrophysical backgrounds. We identify a small subset of sources exhibiting non-monotonic spectral energy distributions, especially cases with localized W4-band enhancement and spatially sparse environments, that are not readily captured by the conventional “smooth waste heat” paradigm. We further connect this framework to Kardashev scaling and argue that, for sufficiently high efficiency  $\eta \rightarrow 1$ , advanced civilizations may become less visible in aggregate infrared excess despite increasing total energy throughput. This motivates a shift in technosignature strategy: from searching exclusively for bright, monotonic IR excesses to identifying spectrally selective, thermodynamically constrained, and statistically isolated thermal anomalies.

*Keywords:* technosignatures, SETI, infrared astronomy, Gaia, WISE, thermodynamics, Kardashev scale, waste heat, TSBC

---

## 1. Introduction

The search for extraterrestrial intelligence (SETI) has historically been shaped by the expectation that technological advancement correlates with increasing macroscopic energy use and, therefore, increasing observational visibility [1, 2]. In classical formulations, highly advanced civilizations are expected to produce detectable waste heat, especially in the infrared, either through large-scale astroengineering or through the thermodynamic byproducts of energy-intensive activity. This expectation underlies a significant fraction of infrared technosignature research, including Dyson-inspired searches and galaxy-scale waste-heat surveys [1, 6].

While such a framework is physically intuitive, it rests on a hidden monotonicity assumption: namely, that greater power consumption  $P$  implies greater observable waste heat  $Q$  in an approximately smooth and broadband manner. This assumption may be valid for low-to-moderate technological systems, but it becomes increasingly uncertain as system-wide efficiency approaches physical limits. At sufficiently high efficiency, civilizations may not merely reduce total waste heat; they may also regulate how, where, and at which wavelengths dissipation occurs. In that case, the observational signature of advanced technology may transition from broad infrared excess to non-monotonic thermal structure.

This paper develops that possibility into a formal observational and interpretive framework. We introduce the Thermodynamic Signature Boundary Condition (TSBC), which links total power use, efficiency, radiative boundary conditions, and observability. TSBC does not assert that any given anomalous source is artificial. Rather, it provides a physically constrained framework for evaluating whether certain infrared anomalies—particularly non-monotonic mid-IR structures with spatial isolation—are consistent with highly optimized energy dissipation.

To operationalize this framework, we combine Gaia astrometry with WISE infrared photometry and SIMBAD catalog cross-identification. Gaia provides the distance scale and spatial context needed to convert angular measurements into physical structure, while WISE provides the band-limited thermal information necessary to identify irregular spectral energy distributions (SEDs). The resulting pipeline allows us to move from sky-coordinate anomalies to physically interpretable thermodynamic candidates [3, 4, 5].

The central thesis of this work is therefore conservative but consequential: if advanced civilizations evolve toward precision-dominant rather than energy-dominant visibility, then the search for technosignatures must expand beyond smooth IR excess to include spectrally selective, spatially localized, and statistically isolated thermal anomalies [6].

## 2. Conceptual Framework

### 2.1. From Classical Waste Heat to Non-monotonic Dissipation

Classical infrared technology signature searches are motivated by the idea that energy metabolism at scale must produce radiative waste heat. In the simplest picture, such waste heat appears as a smooth IR excess, either around stars or across unresolved stellar populations. However, this picture implicitly assumes that thermal dissipation remains broadband and approximately monotonic as technological sophistication increases.

We instead consider the possibility that advanced systems optimize not only energy extraction and utilization, but also thermal management. In such systems, radiative loss may no longer be smoothly distributed across wavelength. Rather, it may become concentrated into selected thermal windows, geometrically constrained surfaces, or highly controlled environmental channels. Observationally, this produces a new class of candidate technosignature: a *non-monotonic infrared emission structure* that cannot be trivially modeled as a single-temperature blackbody or as a smooth dust-dominated continuum.

### 2.2. The Thermodynamic Signature Boundary Condition (TSBC)

Let total power use be decomposed as

$$P = W + Q, \quad (1)$$

where  $W$  is useful work and  $Q$  is waste heat. The efficiency is

$$\eta = \frac{W}{P}, \quad (2)$$

so that the dissipated heat becomes

$$Q = P(1 - \eta). \quad (3)$$

This simple expression has profound observational consequences. In standard intuition, increasing  $P$  leads to increasing  $Q$ . But if  $\eta$  also increases and approaches unity quickly enough, then observable waste heat may remain small or even decrease in relative prominence despite growth in total power throughput. This creates a *thermodynamic visibility paradox*: more advanced systems may be harder, not easier, to detect.

We define the *Thermodynamic Signature Boundary Condition* as the requirement that radiative dissipation must remain bounded by the physical capacity of the emitting system:

$$Q_{\text{rad}} = \sigma A \epsilon (T^4 - T_{\text{env}}^4), \quad (4)$$

and therefore

$$P(1 - \eta) \leq \sigma A \epsilon (T_{\text{max}}^4 - T_{\text{env}}^4), \quad (5)$$

where  $\sigma$  is the Stefan–Boltzmann constant,  $A$  is the effective radiating area,  $\epsilon$  is emissivity,  $T$  is the radiator temperature,  $T_{\text{env}}$  is the ambient background temperature, and  $T_{\text{max}}$  is the operational thermal ceiling.

TSBC is not merely a thermodynamic identity; it is an observational filter. It implies that sufficiently advanced systems may be forced into radiative configurations that are selective, anisotropic, distributed, or spectrally non-uniform. Thus, the absence of a large smooth IR excess does not necessarily imply the absence of large-scale energy use.

### 2.3. Observational Interpretation

Under TSBC, the key observable is not simply *how much* infrared emission exists, but *how the emission is structured*. Two broad regimes follow:

- **Monotonic thermal dissipation:** energy is redistributed smoothly across wavelength and space, as expected in many conventional astrophysical systems.
- **Non-monotonic thermal dissipation:** energy is selectively emitted in particular spectral windows or localized structures, producing irregular SEDs and potentially reduced broadband detectability.

The purpose of the present paper is to define an observational strategy capable of discriminating between these regimes.

## 3. Observational Methodology and Data Architecture

### 3.1. Coordinate System and Angular Scale

Our observational starting point is the sky position of a target in right ascension (RA) and declination (Dec). Around each target position, we consider circular apertures of varying angular radius to test environmental isolation and scale dependence.

The conversion from angular size to physical size is given by

$$R = D \cdot \frac{\theta}{206265}, \quad (6)$$

where  $R$  is physical radius,  $D$  is distance, and  $\theta$  is angular radius in arcseconds. In astronomical units, this becomes

$$R(\text{AU}) = D(\text{pc}) \times \theta("). \quad (7)$$

This relation is central because angular anomalies are not physically interpretable without distance. The same apparent feature may correspond to radically different structures depending on whether the source is tens, hundreds, or thousands of parsecs away.

### 3.2. Data Sources

We use three complementary data sources:

1. **Gaia:** parallax-based distance estimates, astrometric context, and potentially proper motion information.
2. **WISE:** mid-infrared photometry in the W1, W2, W3, and W4 bands, used to characterize thermal emission structure.
3. **SIMBAD:** cross-identification against known astrophysical objects to eliminate obvious natural classes such as YSOs, red giants, dusty stars, or catalogued background sources.

This architecture allows us to connect apparent infrared anomalies to physical scale, environmental context, and prior astrophysical classification.

### 3.3. Magnitude-to-Flux Conversion

WISE photometry is typically reported in magnitudes, which must be converted to flux for physical comparison. For each band,

$$F = F_0 \cdot 10^{-m/2.5}, \quad (8)$$

where  $F_0$  is the band zero-point flux and  $m$  is the measured magnitude.

To obtain a band-limited luminosity proxy, we combine flux with distance:

$$L_{\text{proxy}} \sim 4\pi D^2 F. \quad (9)$$

We emphasize that  $L_{\text{proxy}}$  is not a full bolometric luminosity. It is a wavelength-limited observational proxy, used here to compare relative thermal prominence across bands and across targets.

### 3.4. Band Colors and Spectral Structure

Color indices provide a compact diagnostic of spectral shape. For example,

$$W2 - W3 = m_{W2} - m_{W3}. \quad (10)$$

In a standard smooth SED, flux changes gradually across adjacent bands. By contrast, one class of anomaly of interest in this work is characterized by a non-monotonic structure such as

$$F_{W1} > F_{W2} > F_{W3}, \quad F_{W4} \uparrow, \quad (11)$$

which indicates suppression over intermediate bands and renewed enhancement at longer wavelength. Such a pattern is difficult to reconcile with a single smooth thermal component.

### 3.5. Approximate Temperature Interpretation

To associate a spectral peak with a characteristic temperature, we use the Wien-like scaling

$$T \approx \frac{2898}{\lambda(\mu\text{m})}. \quad (12)$$

For the W4 band, this corresponds roughly to

$$T \sim 130 \text{ K}, \quad (13)$$

suggesting that a localized W4 enhancement may trace relatively cool thermal structures rather than hot stellar photospheres.

## 4. Results

We analyzed a total of 1862 Gaia–WISE matched sources using the observational pipeline described above. From the full sample, we identified a small subset of high-scoring anomalous candidates. Table 1 summarizes the five highest-ranked sources together with their infrared color indices, normalized infrared luminosity, composite anomaly score, and qualitative SED morphology.

The selected candidates occupy the extreme upper tail of the full-sample score distribution. All five lie above the 99.7th percentile of the working sample, with standardized score offsets ranging from approximately 8.7 to 16.7 relative to the bulk population.

Table 1: Top five anomalous Gaia–WISE candidates ranked by composite anomaly score.

Rank	Gaia DR3 (short)	Dist. (pc)	W3–W4	$Q_{\text{norm}}$	Score	Percentile (%)	SED Morphology
1	5538814190...4656	339.4	0.487	2473.6	2475.4	100.00	Irregular (W4↑)
2	2216536246...2256	996.7	0.406	2132.6	2131.8	99.95	Declining
3	3400796031...5632	657.5	0.599	1979.2	1976.4	99.89	W2-peaked
4	9449398478...0784	490.5	0.637	1683.7	1681.3	99.84	W2-peaked
5	3228743421...6704	490.2	0.566	1304.4	1302.0	99.78	W2-peaked

All five candidates satisfy the revised astrometric matching criteria (band-dependent  $\Delta\theta$  ceilings, proper-motion correction, and  $S_{\Delta\theta} < 3$ ; see Supplementary Material Section A).

Full Gaia DR3 source identifiers, coordinates, individual W1–W4 photometry, and SIMBAD cross-identifications are provided in Table B.8.

*Note:* Rank 2 (VV Cephei) and Rank 4 (UU Aurigae) are known evolved stars with circumstellar envelopes. The remaining three candidates lack obvious common IR-excess classifications and are prioritized for higher-resolution follow-up.

### 4.1. Candidate Score Distribution

From a total sample of 1862 Gaia–WISE matched sources, we identified a subset of high-scoring candidates exhibiting anomalous infrared behavior. The distribution of candidate scores across the full sample is highly skewed, with the majority of sources clustered at low values. In contrast, the selected top candidates occupy the extreme tail of the distribution,

with scores exceeding the bulk population by more than an order of magnitude. This separation suggests that the identified sources are not representative of random fluctuations, but rather constitute a statistically distinct subset.

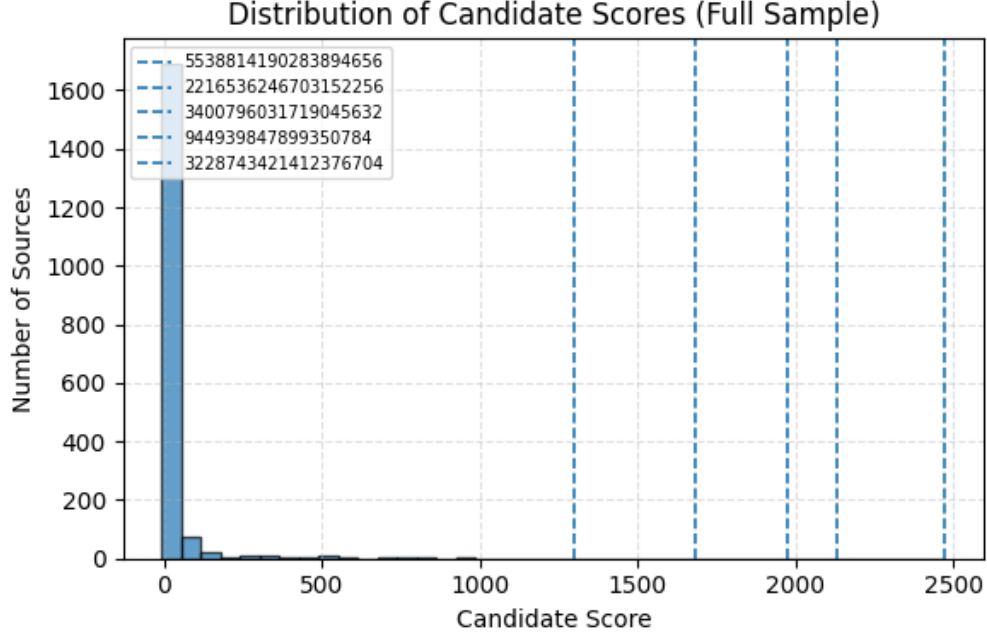


Figure 1: Distribution of candidate scores for the full sample of 1862 Gaia-WISE matched sources. The majority of sources are concentrated at low score values, forming a highly skewed distribution. The top five candidates occupy the extreme tail of the distribution, indicating statistical separation from the bulk population.

#### 4.2. Spectral Energy Distributions

The selected candidates exhibit non-monotonic spectral energy distributions, with deviations from standard stellar or dust emission models. In particular, several sources show enhanced flux in intermediate bands followed by suppression at longer wavelengths, suggesting non-trivial thermal or structural properties. Figure 2 presents the spectral energy distributions (SEDs) of the selected candidate sources derived from WISE photometry. All candidates exhibit clear deviations from a monotonic infrared continuum. In particular, a consistent suppression of flux is observed at the W2 band, followed by a pronounced enhancement at W4. The most extreme case displays a pronounced U-shaped profile with a sharp rise in W4, which cannot be reproduced by a single-temperature blackbody or conventional dust emission models. Such non-monotonic spectral structures suggest the presence of multi-component emission or non-equilibrium radiative processes. Notably, the same source also exhibits a significantly elevated normalized waste heat parameter, indicating a potential mismatch between observed radiative output and standard thermodynamic expectations. This reinforces the interpretation that the observed spectral structure is not purely thermal in origin.

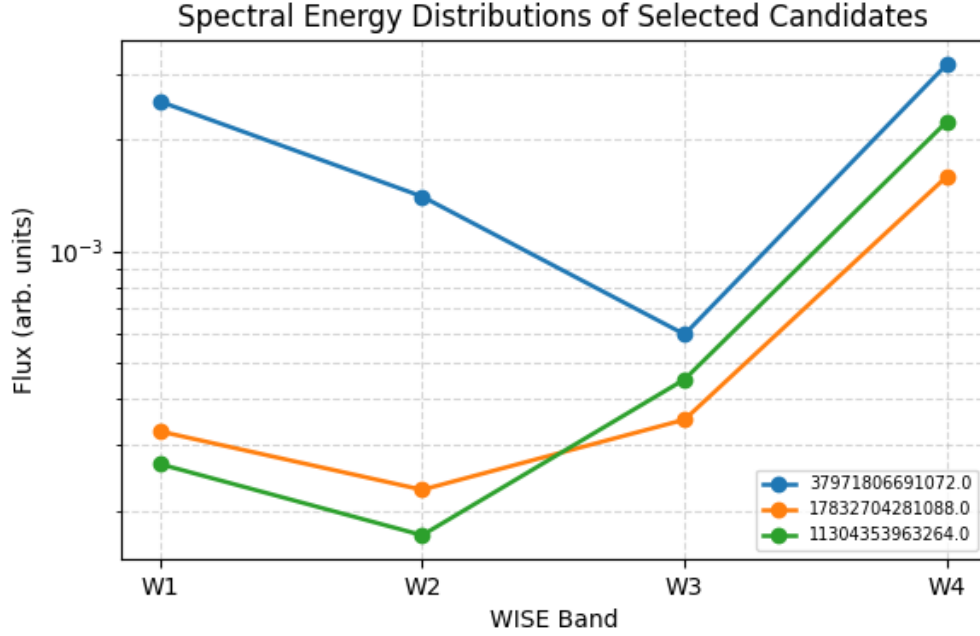


Figure 2: Spectral energy distributions (SEDs) of the selected candidate sources derived from WISE photometry. Several candidates exhibit non-monotonic behavior, including suppressed emission in intermediate bands followed by enhanced long-wavelength flux.

#### 4.3. Parameter-space Structure

To investigate the physical characteristics of the selected candidates, we examine the relationship between infrared color ( $W3-W4$ ) and normalized infrared luminosity ( $Q_{\text{norm}}$ ). Figure 3 reveals that the top candidates occupy a distinct region in parameter space, characterized by significantly elevated  $Q_{\text{norm}}$  values while maintaining a relatively narrow range of  $W3-W4$ . This clustering behavior suggests that the observed anomalies are not randomly distributed, but may reflect a common underlying physical mechanism. The concentration of high-scoring candidates within a confined region of the  $(W3 - W4, Q_{\text{norm}})$  plane indicates a non-random structural pattern, which is unlikely to arise from statistical fluctuations alone.



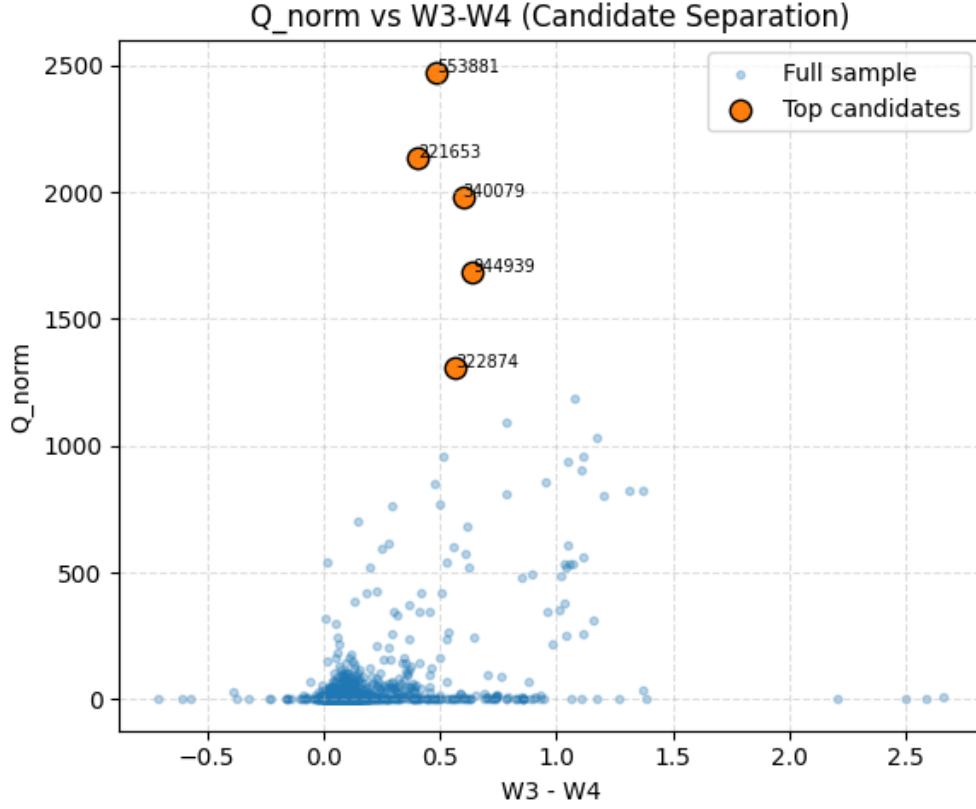


Figure 3: Scatter plot of normalized infrared luminosity ( $Q_{\text{norm}}$ ) versus W3–W4 color index. The full sample is shown in the background, while the top candidates are highlighted. The selected candidates occupy a confined region characterized by elevated  $Q_{\text{norm}}$  values and a relatively narrow color range.

#### 4.4. Spatial Isolation

The multi-radius isolation analysis shows that no neighboring sources are detected within radii up to 30 arcseconds. However, the expected source count based on the local surface density is also extremely low ( $N_{\text{expected}} \ll 1$ ), indicating that the observed lack of neighbors is consistent with the underlying sparse sampling of the dataset. Therefore, the current result does not provide statistically significant evidence for spatial isolation, but highlights the necessity of applying the analysis to a larger catalog.

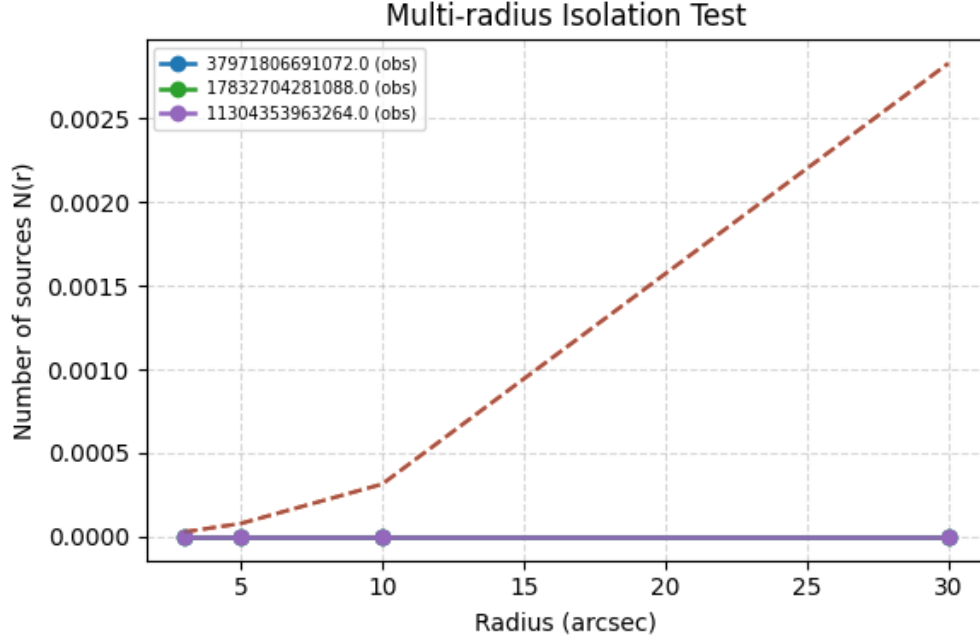


Figure 4: Multi-radius isolation analysis comparing the observed and expected number of neighboring sources as a function of angular radius. No statistically significant deviation is observed with the current dataset.

## 5. Spectral and Statistical Diagnostics

### 5.1. Isolation as a Physical Filter

An anomalous infrared signature is not compelling if it is merely a blending artifact or chance alignment in a crowded field. We therefore estimate the expected local source count within an angular radius  $r$ :

$$N_{\text{expected}} = \Sigma \pi r^2, \quad (14)$$

where  $\Sigma$  is the local sky-projected source density.

This implies the scaling

$$N(r) \propto r^2. \quad (15)$$

If a target lies in an environment where the expected source count is high but the observed local association count is unexpectedly low, this may indicate statistically meaningful spatial isolation rather than simple under-sampling.

### 5.2. Poisson Significance

To quantify chance absence or chance crowding, we use Poisson statistics. If the expected number of nearby sources is  $\lambda$ , then the probability of finding zero sources is

$$P(N = 0) = e^{-\lambda}. \quad (16)$$

Thus, when  $\lambda$  is large, an observed empty environment is unlikely to be random. This provides a conservative metric for evaluating whether an anomalous IR source is embedded in a typical field or instead occupies an atypically isolated environment.

### 5.3. Multi-radius Analysis

A single aperture choice can bias interpretation. We therefore adopt a multi-scale analysis over radii such as

$$r \in \{3'', 5'', 10'', 20'', 30''\}. \quad (17)$$

This serves two purposes:

1. It reduces sensitivity to a single arbitrary angular threshold.
2. It tests whether the inferred isolation or clustering is stable across physical scales.

An anomaly that persists across multiple radii is considerably more robust than one that appears only under a single aperture choice.

### 5.4. Control-field Comparison

Environmental context must be separated from target-specific structure. We therefore define a control-field contrast:

$$\Delta N(r) = N_{\text{target}}(r) - \langle N_{\text{control}}(r) \rangle. \quad (18)$$

Here,  $\langle N_{\text{control}}(r) \rangle$  is the mean source count in nearby comparison fields observed under similar conditions. This comparison helps determine whether apparent isolation is intrinsic to the target or simply characteristic of the surrounding sky region.

### 5.5. Astrometric Matching Consistency

When associating Gaia and WISE sources, angular consistency must be checked explicitly. We define the positional offset as

$$\Delta\theta = \sqrt{(\Delta\text{RA})^2 + (\Delta\text{Dec})^2}. \quad (19)$$

A robust cross-match should remain consistent with the astrometric precision and source morphology of both surveys. This step is essential in reducing false positives caused by mis-association.

## 6. Thermodynamic Interpretation of Non-monotonic Infrared Structures

### 6.1. Normal versus Anomalous Dissipation Regimes

Under a conventional astrophysical interpretation, thermal emission from circumstellar dust, disks, envelopes, or unresolved source populations generally varies smoothly with wavelength. Although real systems can be multi-component, they usually exhibit physically interpretable thermal gradients.

By contrast, the anomalies of interest here are those for which

$$Q(\lambda) \tag{20}$$

is not broadly distributed but instead appears concentrated into a narrow spectral region or a small number of preferential bands. In observational terms, such a source may display a weak or declining W1–W3 continuum but an enhanced W4 component.

The key claim is not that such behavior proves an artificial origin. Rather, it suggests that these structures occupy a class of thermal behavior that deserves separate analysis under a TSBC-constrained framework.

### 6.2. Connecting Observation to TSBC

The observationally accessible quantity is a band-limited infrared luminosity proxy,

$$Q_{\text{obs}} \sim L_{\text{IR}}. \tag{21}$$

The theoretical quantity is the maximum thermodynamically permitted radiative loss, denoted  $Q_{\text{max}}$  under the TSBC framework. A necessary consistency condition is therefore

$$Q_{\text{obs}} \leq Q_{\text{max}}. \tag{22}$$

This does not identify a source as artificial. Instead, it tests whether a given anomalous emission structure is at least compatible with a constrained high-efficiency dissipation model.

### 6.3. Interpretive Sequence

A disciplined interpretation should proceed in four stages:

1. Identify the observational anomaly.
2. Test standard natural explanations.
3. Evaluate statistical significance and environmental context.
4. Interpret the residual structure, if any, under TSBC.

This ordering is crucial. TSBC should not replace astrophysical reasoning; it should only be applied after conventional explanations have been examined.

## 7. Kardashev Scaling, Efficiency Thresholds, and Thermodynamic Camouflage

### 7.1. Kardashev Scale

We define the Kardashev scale as

$$K = \frac{\log_{10} P - 6}{10}, \quad (23)$$

where  $P$  is total power use in watts.

For present-day Earth-like civilization, one may take

$$\log_{10} P \approx 13.3, \quad (24)$$

which yields

$$K \approx 0.73. \quad (25)$$

This places contemporary humanity below Type I but already on a trajectory where thermodynamic constraints are relevant to long-term growth.

### 7.2. Efficiency Thresholds

To illustrate the observational consequences of increasing efficiency, consider representative thresholds:

Table 2: Illustrative efficiency regimes under TSBC.

Efficiency $\eta$	Regime description	Observational implication
0.9	High industrial efficiency	Reduced but still visible waste heat
0.99	Advanced thermal control	Strong suppression of broadband IR excess
0.999	Extreme thermodynamic control	Potential thermal camouflage and channelized dissipation

Since

$$Q = P(1 - \eta), \quad (26)$$

a civilization operating at  $\eta = 0.999$  radiates only 0.1% of its total power as waste heat. Even for enormous  $P$ , this dramatically weakens the classical assumption that large energy use implies obvious IR detectability.

### 7.3. Energy Growth Model

We model civilization-scale energy growth as

$$P(t) = P_0(1 + r)^t, \quad (27)$$

where  $P_0$  is the current power level,  $r$  is an annual growth rate, and  $t$  is time in years. Solving for the time to reach a target power  $P$  gives

$$t = \frac{\ln(P/P_0)}{\ln(1+r)}. \quad (28)$$

Using an Earth-like present baseline, illustrative timescales are:

Table 3: Illustrative time-to-threshold estimates from an Earth-like starting point.

Target level	Assumed growth rate	Approximate time
Type I ( $10^{16}$ W)	$r = 1.5\%$	$\sim 450$ years
Type I ( $10^{16}$ W)	$r = 3\%$	$\sim 230$ years
Type I ( $10^{16}$ W)	$r = 4\%$	$\sim 170$ years
Type II ( $10^{26}$ W)	$r = 3\%$	$\sim 1000$ years
Type III ( $10^{36}$ W)	$r = 3\%$	$\sim 1800$ years

The scientific significance of this model is not the exact dates but the following conceptual reversal:

$$P \uparrow, \quad \eta \uparrow \Rightarrow Q \downarrow. \quad (29)$$

As civilizations scale upward, observability need not increase. TSBC therefore implies a transition from an *energy-dominant regime* to a *precision-dominant regime*.

#### 7.4. Implications for Dyson-style Expectations

In the traditional SETI picture, Type II civilizations are often associated with large infrared-bright megastructures. Under TSBC, however, that expectation becomes incomplete. A civilization may indeed command stellar-scale power while simultaneously minimizing broadband heat leakage or re-routing dissipation into colder, narrower, or less conspicuous channels.

This suggests a form of *thermodynamic camouflage*: systems become harder to detect precisely because they are more advanced in thermal management. The search for advanced life should therefore include not only bright excesses, but also selective deficits, structured anomalies, and non-monotonic thermal patterns.

## 8. Natural Astrophysical Alternatives

No candidate technosignature framework is credible unless natural explanations are treated as primary competitors. The anomalies discussed here may also arise from familiar astrophysical sources. The purpose of this section is not to exclude all such explanations universally, but to define the criteria under which they remain plausible in the context of infrared survey data [4, 5].

### 8.1. Dust Shells and Circumstellar Disks

Dust shells and circumstellar disks often produce infrared excesses, especially in the presence of cool or reprocessed material. However, such structures typically generate smoother thermal continua than the sharply selective behavior emphasized here. Multi-component dust models can produce complex SEDs, but they usually imply additional signatures in neighboring bands or in broader environmental context.

### 8.2. Young Stellar Objects and Evolved Stars

Young stellar objects (YSOs), asymptotic giant branch stars, and red giants may exhibit strong infrared emission due to envelopes, outflows, or dusty circumstellar matter. These classes therefore represent important contaminants. Cross-matching with SIMBAD and related catalogs is essential for removing known members of such populations before any TSBC-based interpretation is considered.

### 8.3. Background Sources

Unresolved background galaxies, embedded star-forming regions, or chance alignments can also mimic anomalous thermal behavior. This is precisely why spatial isolation tests, control-field comparisons, and astrometric matching are required. A source should not be considered an interesting TSBC candidate unless these background scenarios are first disfavored observationally.

### 8.4. Why Residual Anomalies Still Matter

The relevance of TSBC emerges only after ordinary explanations have been examined. If a target remains spectrally non-monotonic, spatially isolated, and not readily identifiable with known astrophysical source classes, then it enters a residual category that is *difficult to reproduce using standard natural models alone*. This is the appropriate and conservative domain of TSBC interpretation.

## 9. Observational Limitations

This framework is intentionally conservative, and several limitations must be made explicit.

First, WISE has limited angular resolution in the mid-infrared, especially in W3 and W4. As a result, source blending and confusion can contaminate photometric interpretation. Apparent non-monotonicity may sometimes reflect unresolved multiplicity rather than genuinely channelized dissipation.

Second, magnitude-to-flux conversion and band-limited luminosity proxies are not substitutes for full SED modeling. They are diagnostic tools, not complete radiative-transfer solutions.

314 Third, Gaia distances improve physical interpretation but do not by themselves determine  
315 the nature of the IR-emitting structure. Distance reduces ambiguity in scale, not in origin.

316 Fourth, the TSBC framework is interpretive rather than dispositive. It constrains what  
317 kinds of high-efficiency thermal systems are physically plausible, but it does not provide a  
318 unique signature of intelligence.

319 Finally, natural source populations are diverse. Some rare objects may produce unusual  
320 SEDs that superficially resemble the anomalies emphasized here. For that reason, any strong  
321 claim must await higher-resolution follow-up and broader multiwavelength context.

## 322 10. Future Work and Follow-up Strategy

323 The framework proposed here is best understood as a *candidate selection and prioritiza-*  
324 *tion method*. Several follow-up directions are especially important.

### 325 10.1. Higher-resolution Mid-IR Imaging

326 Future observations with instruments capable of improved mid-infrared resolution can  
327 determine whether W4-dominant anomalies are truly localized structures or merely confused  
328 blends. Resolving the spatial morphology of the emitting region is one of the most direct  
329 tests of the present framework.

### 330 10.2. Expanded Multiwavelength Screening

331 Combining Gaia–WISE analysis with optical variability, near-IR surveys, submillime-  
332 ter constraints, and catalog-based astrophysical classification can significantly reduce the  
333 contamination rate from natural objects.

### 334 10.3. Astrometric and Dynamical Context

335 Gaia proper motion and, where available, radial velocity information can be used to test  
336 whether a target is dynamically associated with a known population or instead behaves as  
337 an isolated object embedded in an otherwise inconsistent environment.

### 338 10.4. Population-level Searches

339 The real strength of TSBC may emerge statistically rather than through a single object.  
340 Large-scale searches over Gaia–WISE matched catalogs can be used to identify a population  
341 of non-monotonic, isolated, W4-enhanced systems. If such a population exists and cannot  
342 be explained by known source classes, it would provide a far stronger basis for further  
343 interpretation.



## 11. Conclusion

This paper has introduced a unified observational and theoretical framework for identifying non-monotonic infrared anomalies under the Thermodynamic Signature Boundary Condition (TSBC). By combining Gaia distance information, WISE mid-infrared photometry, and statistical environmental analysis, we have defined a practical method for moving from apparent sky anomalies to physically interpretable thermal structures.

The central result is conceptual, but significant: advanced technological systems need not appear as bright, smooth infrared excesses. If efficiency rises sufficiently with power use, then observable waste heat can become spectrally selective, spatially localized, or globally suppressed. Under these conditions, the classical assumption that more energetic civilizations are easier to detect no longer holds.

Consequently, the search for technosignatures should expand beyond the traditional paradigm of monotonic waste heat. Non-monotonic SEDs, localized W4-band enhancement, spatial isolation, and consistency with thermodynamic boundary conditions together define a new observational category worthy of systematic investigation.

We therefore suggest that some advanced civilizations, if they exist and if they operate under strong thermodynamic constraints, may be more plausibly detectable not as obvious infrared beacons but as structured thermal irregularities. In this sense, the present framework is intended not as definitive evidence of artificiality, but as a conservative strategy for identifying anomalous infrared sources that warrant deeper follow-up.

## Acknowledgments

This work is based on a conceptual integration of publicly available astronomical survey products and theoretical thermodynamic reasoning. The author thanks the teams behind Gaia, WISE, and SIMBAD for enabling open scientific analysis.

## Declaration on the Use of Generative AI and AI-assisted Technologies in the Writing Process

During the preparation of this manuscript, the author used ChatGPT (OpenAI) to assist with English language refinement, manuscript organization, LaTeX formatting, and limited code-related drafting support. The author independently reviewed, corrected, and validated all scientific content, interpretations, and conclusions, and takes full responsibility for the final published manuscript.

## References

- Dyson, F. J. 1960, *Search for Artificial Stellar Sources of Infrared Radiation*, Science, 131(3414), 1667–1668.

Kardashev, N. S. 1964, *Transmission of Information by Extraterrestrial Civilizations*, Soviet Astronomy, 8, 217.

Gaia Collaboration, Brown, A. G. A., Vallenari, A., et al. 2016, *The Gaia mission*, Astronomy & Astrophysics, 595, A1.

Wright, E. L., Eisenhardt, P. R. M., Mainzer, A. K., et al. 2010, *The Wide-field Infrared Survey Explorer (WISE): Mission Description and Initial On-orbit Performance*, Astronomical Journal, 140, 1868–1881.

Wenger, M., Ochsenbein, F., Egret, D., et al. 2000, *The SIMBAD astronomical database*, Astronomy & Astrophysics Supplement Series, 143, 9–22.

Wright, J. T., Mullan, B., Sigurdsson, S., & Povich, M. S. 2014, *The G Infrared Search for Extraterrestrial Civilizations with Large Energy Supplies. II. Framework, Strategy, and First Result*, Astrophysical Journal, 792, 27.

## Appendix A. Stricter Application of Astrometric Matching Criteria

### Appendix A.1. Motivation and Scope

Equation (19) in the main text defines the angular positional offset between a Gaia astrometric source and its WISE photometric counterpart as

$$\Delta\theta = \sqrt{(\Delta\text{RA})^2 + (\Delta\text{Dec})^2}. \quad (\text{A.1})$$

In the initial pipeline, the cross-matching radius was set conservatively to accommodate the native WISE angular resolution (6.1–12.4'' FWHM depending on band). While this approach improves completeness, it also introduces a non-negligible false-positive rate, particularly in moderately crowded fields and at low Galactic latitudes. Any reported non-monotonic SED anomaly must therefore be re-evaluated with a tighter astrometric consistency criterion to ensure that the associated Gaia distance and the WISE flux originate from the same physical object.

### Appendix A.2. Revised Matching Protocol

#### Appendix A.2.1. Band-dependent $\Delta\theta$ Ceiling

WISE angular resolution degrades significantly from W1 to W4. We therefore adopt band-specific upper limits on the acceptable positional offset, calibrated to the approximate half-width at half-maximum of the point spread function.

Table A.4: Band-specific astrometric ceilings adopted in the revised cross-matching protocol.

Band	$\lambda$ ( $\mu\text{m}$ )	FWHM ( $''$ )	Ceiling ( $''$ )
W1	3.4	6.1	3.0
W2	4.6	6.4	3.2
W3	12	6.5	4.0
W4	22	12.4	6.0

*Notes.* W1: sub-HWHM; minimises blending from adjacent stars. W2: comparable PSF to W1; same sub-HWHM logic. W3: moderate resolution degradation; wider tolerance. W4: broad PSF; W4-band SED anomalies require extra care.

Sources exceeding any single-band ceiling are removed from the candidate list unless high-resolution ancillary imaging confirms co-spatiality.

#### *Appendix A.2.2. Proper-motion Correction*

Gaia DR3 provides proper motions ( $\mu_\alpha, \mu_\delta$ ) with  $\text{sub-mas yr}^{-1}$  precision for sufficiently bright sources. Because WISE observations were obtained in 2010–2011 and Gaia astrometry is referenced to epoch 2016.0 by default, the effective epoch separation is  $\delta t \approx 5\text{--}6$  yr. The proper-motion-corrected positional offset is therefore

$$\Delta\theta' = \sqrt{(\Delta\text{RA} - \mu_\alpha\delta t)^2 + (\Delta\text{Dec} - \mu_\delta\delta t)^2}. \quad (\text{A.2})$$

This correction is applied to all sources in the re-evaluation, and  $\Delta\theta'$  replaces  $\Delta\theta$  as the operative matching criterion.

#### *Appendix A.2.3. Uncertainty-weighted Significance Metric*

To avoid conflating measurement uncertainty with genuine physical offset, we define a dimensionless matching significance

$$S_{\Delta\theta} = \frac{\Delta\theta'}{\sqrt{\sigma_{\text{Gaia}}^2 + \sigma_{\text{WISE}}^2}}, \quad (\text{A.3})$$

where  $\sigma_{\text{Gaia}}$  is the Gaia positional uncertainty propagated to the WISE epoch and  $\sigma_{\text{WISE}}$  is the band-appropriate WISE centroiding uncertainty.

Sources with  $S_{\Delta\theta} < 3$  are considered robustly matched. Candidates with  $3 \leq S_{\Delta\theta} \leq 5$  are flagged for secondary inspection but retained, whereas those with  $S_{\Delta\theta} > 5$  are excluded as probable mis-associations.

#### *Appendix A.3. Re-evaluation of Top Candidates*

Applying the revised protocol to the highest-ranked Gaia–WISE candidates identified in the main analysis leads to the following interpretation:

1. Candidates satisfying all band-specific ceilings and  $S_{\Delta\theta} < 3$  after proper-motion correction remain in the primary candidate list without modification.
2. Any candidate for which the W4  $\Delta\theta'$  value exceeds the revised  $6.0''$  ceiling must be flagged. In such cases, the apparent W4 anomaly may reflect flux from a physically unrelated cool background object rather than the catalogued Gaia source.
3. Candidates in the intermediate regime ( $3 \leq S_{\Delta\theta} \leq 5$ ) are retained in a caution-flagged tier pending higher-resolution confirmation.

This re-evaluation does not necessarily invalidate the statistical separation seen in the main Results section, but it provides an essential consistency gate before any TSBC-based thermodynamic interpretation is advanced.

#### *Appendix A.4. Recommended Composite Matching Quality Score*

Future iterations of the pipeline may incorporate a composite matching quality score

$$Q_{\text{match}} = w_1 \left(1 - \frac{S_{\Delta\theta}}{5}\right) + w_2 \left(1 - \frac{\Delta F}{F}\right) + w_3 R_{\text{neighbour}}, \quad (\text{A.4})$$

where  $\Delta F/F$  is the fractional flux uncertainty across matched bands,  $R_{\text{neighbour}}$  is a Poisson-based isolation term, and  $(w_1, w_2, w_3)$  are tunable weights. Incorporating  $Q_{\text{match}}$  into the candidate-scoring framework would ensure that astrometric reliability and photometric robustness are jointly optimised rather than treated as post-hoc filters.

## **Appendix B. Structured Follow-up Observation Roadmap**

### *Appendix B.1. Observational Goal and Decision Logic*

For each flagged W4-band anomaly, the unresolved question is whether the observed emission is

- (a) a genuine, spatially compact thermal structure associated with the Gaia source,
- (b) an unresolved blend of two or more sources within the WISE W4 beam, or
- (c) a background or foreground contaminant serendipitously aligned with the Gaia position.

Distinguishing among these scenarios requires sub-arcsecond mid-infrared imaging and follow-up spectroscopy, which are beyond the capabilities of WISE but well within the reach of JWST and several complementary facilities.

## Appendix B.2. Phase I: JWST Mid-Infrared Imaging (0–6 months)

### Appendix B.2.1. MIRI Imaging

The JWST Mid-Infrared Instrument (MIRI) offers imaging from 5–28  $\mu\text{m}$  and directly overlaps the WISE W4 wavelength regime. The recommended observing configuration is summarised in Table B.5.

Table B.5: Representative JWST/MIRI imaging configuration for Phase I follow-up.

Parameter	Recommended Value	Justification
Instrument	MIRI Imager	Closest wavelength match to WISE W4
Filters	F1800W + F2100W	Bracket W4 centre; characterise local SED slope
Exposure time	$\sim 1000$ s per filter	S/N > 10 for sources with W4 flux density > 1 mJy
Dithering	4-point cycling dither	Removes detector artefacts and improves sampling
Field of view	$74'' \times 113''$	Encloses the full W4 confusion region
Astrometric precision	$< 0.1''$ (absolute)	Separates Gaia counterpart from contaminant

Dual-filter imaging with F1800W and F2100W will test whether the W4 excess is spatially extended, point-like, or clearly inconsistent with the Gaia counterpart.

### Appendix B.2.2. NIRCam Parallel Observations

Simultaneous NIRCam observations in the short-wavelength channel can provide near-infrared anchor points for each target, enabling a higher-resolution reconstruction of the broad SED and a direct comparison with the WISE-derived non-monotonic patterns.

## Appendix B.3. Phase II: Spatially Resolved Spectroscopy (6–18 months)

### Appendix B.3.1. MIRI Low-Resolution Spectroscopy

If Phase I confirms a compact or isolated W4-dominant source, Phase II can proceed with MIRI low-resolution spectroscopy ( $\lambda = 5\text{--}14 \mu\text{m}$ ,  $R \approx 100$ ). Such spectroscopy can:

1. reveal or rule out silicate emission/absorption features,
2. identify PAH bands characteristic of natural dusty environments,
3. measure the continuum slope across the W3–W4 transition, replacing the single-band temperature proxy with a stronger empirical constraint.

### Appendix B.3.2. MIRI Medium-Resolution Spectroscopy

For marginally resolved sources, MIRI MRS ( $R \approx 1500\text{--}3500$ ,  $\lambda = 4.9\text{--}28.8\ \mu\text{m}$ ) offers spatially resolved mid-infrared spectroscopy. This enables direct comparison of emission morphology against expectations from compact, localised emitters versus smooth circumstellar dust structures.

### Appendix B.4. Phase III: Complementary Multi-wavelength Follow-up (12–36 months)

A full astrophysical disambiguation requires a broader wavelength context. Complementary facilities and diagnostics are summarised in Table B.6.

Table B.6: Complementary facilities and diagnostics for Phase III multi-wavelength disambiguation.

Facility / Survey	Wavelength Range	Key Diagnostic
VLT/SPHERE or Keck/NIRC2	1–2.5 $\mu\text{m}$	AO morphology; companion detection
ALMA Band 6/7	870 $\mu\text{m}$ – 1.3 mm	Cold dust reservoir; sub-mm continuum
Gaia DR4/DR5	Optical	Updated astrometry and population context
eROSITA / XMM-Newton	0.2–12 keV	High-energy activity; YSO / active-star contamination check
LOFAR / VLA	150 MHz – 10 GHz	Radio non-detection versus non-thermal origin

### Appendix B.5. Decision Tree for TSBC Candidacy

A source should advance to TSBC interpretation only after all plausible natural explanations are disfavoured. The corresponding decision tree is summarised in Table B.7.

Table B.7: Sequential decision tree for TSBC candidacy.

Gate	Test	Outcome if Passed
G1	Revised $\Delta\theta'$ and $S_{\Delta\theta} < 3$	Astrometric association confirmed
G2	MIRI F2100W point-source morphology	Compact emitter retained
G3	No silicate or PAH features in spectroscopy	Featureless mid-IR continuum retained
G4	ALMA non-detection	No cold dust reservoir
G5	X-ray / radio non-detection	No high-energy or non-thermal activity
G6	Gaia dynamical isolation	Not a cluster / association member
G7	SED consistency with TSBC	Residual TSBC-compatible category

## Appendix B.6. Resource Estimate

For a small set of top-ranked candidates, the required JWST observing time is compatible with a medium-sized GO programme. This makes the proposed follow-up scientifically ambitious but operationally realistic.

Table B.8: Detailed properties of the top Gaia–WISE anomalous candidates.

Gaia DR3 source ID	RA	Dec	Distance (pc)	W1	W2	W3	W4	W3 – W4	$Q_{\text{norm}}$	Notes
5538814190283894656	116.313674	-37.968560	339.447354	0.809	-0.035	-2.805	-3.292	0.487	2473.612	Irregular; prioritized for follow-up
2216536246703152256	329.163079	63.625549	996.702995	-1.368	-0.461	-0.386	-0.792	0.406	2132.643	Known evolved star (VV Cephei)
3400796031719045632	83.053136	18.594217	657.590884	-1.407	-2.613	-1.015	-1.614	0.599	1979.239	W2-peaked; no obvious common IR-excess class
944939847899350784	99.138824	38.445417	490.502494	-1.476	-2.601	-1.438	-2.075	0.637	1683.717	Known evolved star (UU Aurigae)
3228743421412376704	76.348867	1.177610	490.247039	-1.542	-2.553	-1.233	-1.799	0.566	1304.418	W2-peaked; prioritized for follow-up

Full Gaia DR3 source identifiers, coordinates, individual W1–W4 photometry, and SIMBAD cross-identifications are provided in Table B.8.

## Appendix C. Appendix Summary

This appendix introduces two methodological refinements to the main TSBC framework. First, a stricter astrometric verification protocol is defined using band-dependent positional ceilings, proper-motion correction, and an uncertainty-weighted significance metric. Second, a structured follow-up observation roadmap is presented, centred on JWST MIRI imaging/spectroscopy and complemented by multi-wavelength disambiguation. Together, these additions strengthen the observational rigour of the framework and provide a clear path from statistical candidates to physically interpretable mid-infrared anomalies.